APPLIED ORGANOMETALLIC CHEMISTRY
Appl. Organometal. Chem. 2002; **16**: 617–627
Materials, Nanomaterials and Synthesis AOC
Published online in Wiley InterScience (www.interscience.wiley.com). DOI:10.1002/aoc.362

Ternary single-source precursors for polycrystalline thin-film solar cells

Kulbinder K. Banger[1], Jennifer A. Hollingsworth[2], Jerry D. Harris[3], Jonathan Cowen[3], William E. Buhro[2] and Aloysius F. Hepp[4]*

[1]Ohio Aerospace Institute, 22800 Cedar Point Road, Cleveland, OH 44142, USA
[2]Department of Chemistry, Washington University, One Brookings Drive, St Louis, MO 63130, USA
[3]Department of Chemistry, Cleveland State University, Cleveland, OH 44115, USA
[4]Photovoltaic & Space Environments Branch, NASA Glenn Research Center, Cleveland, OH 44135, USA

Received 15 April 2002; Accepted 5 June 2002

The development of thin-film solar cells on flexible, lightweight, space-qualified substrates provides an attractive cost solution for fabricating solar arrays with high specific power (W kg^{-1}). The use of a polycrystalline chalcopyrite absorber layer for thin-film solar cells is considered as the next generation in photovoltaic devices. At NASA GRC we have focused on the development of new single-source precursors (SSPs) and their utility to deposit the chalcopyrite semiconducting layer (CIS) onto flexible substrates for solar-cell fabrication. The syntheses and thermal modulation of SSPs via molecular engineering are described. Thin-film fabrication studies demonstrate that the SSPs can be used in a spray chemical vapor deposition process for depositing CIS at reduced temperatures, and result in electrical properties that are suitable for photovoltaic devices. Copyright © 2002 John Wiley & Sons, Ltd.

INTRODUCTION

The development of thin film flexible lightweight solar cells is of high importance for both terrestrial and space applications. Thin-film solar cells use 30–100 times less semiconducting material and are less expensive to manufacture than conventional crystalline silicon cells. Current thin-film photovoltaic (PV) research encompasses development of CdTe, Cu(Ga:In)(S:Se)$_2$ (CIS), and thin film silicon-based solar cells. One of the most promising technologies lies in the development of polycrystalline thin films,[1] due to their ease of manufacture and, importantly, their lightweight structure, which enables them to achieve higher specific power (W kg^{-1}) than alternative single crystalline devices.[2]

With the increasing cost of launching payloads into space, currently estimated to be approximately $20k per kilogram, lightweight materials for space power systems are now being considered. Use of flexible solar cells will be mission enabling for several proposed NASA space programs, which allows for efficient storage in launch vehicles for later controlled deployment in space (Fig. 1). Similarly, for terrestrial applications, thin-film PVs are highly appealing due to their flexible lightweight construction, permitting them to be 'molded' onto non-rigid, or uniform structures for off-grid or innovative power systems.

PV modules based on ternary chalcopyrite absorber layers, (I–III–VI$_2$; Cu(In:Ga)(S:Se)$_2$) have been the focus of extensive investigation for over two decades. The use of chalcopyrite absorbers is highly appealing, since their bandgaps correlate well to the maximum photon power density in the solar spectrum for both terrestrial (AM1.5), and space applications (AM0) (Fig. 2), while displaying long-term stability and excellent radiation tolerance.[3–5] Additionally, by adjusting the percent atomic composition of either galium for indium and/or sulfur for selenium, the bandgap

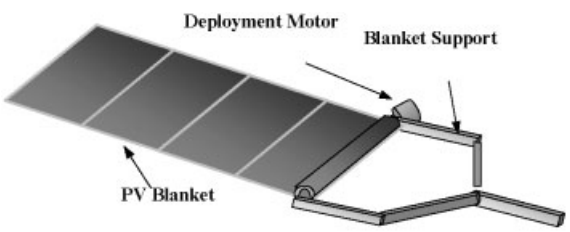

Figure 1. Lightweight flexible PV array.

*Correspondence to: A. F. Hepp, NASA Glenn Research Center, 21000 Brookpark Road, Mail Stop 302-1, Cleveland, OH 44135, USA.
E-mail: aloysius.f.hepp@grc.nasa.gov
Contract/grant sponsor: NASA; Contract/grant number: NCC3-817; Contract/grant number: NCC3-563; Contract/grant number: NCC3-734.

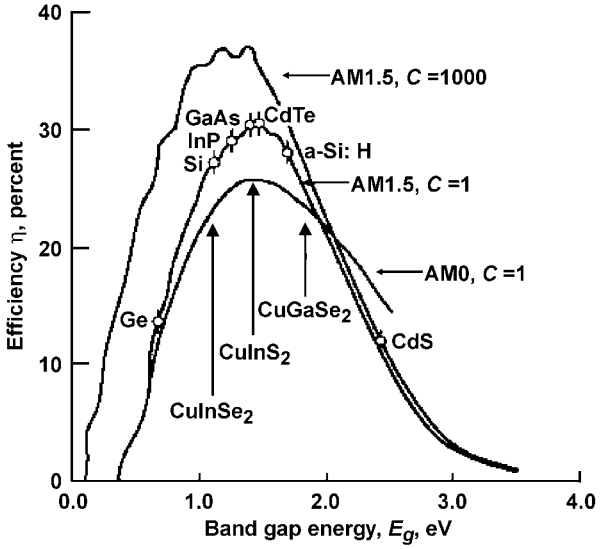

Figure 2. Predicted efficiency versus bandgap for thin-film PV materials for solar spectra in space (AM0) and on the surface of the Earth (AM1.5) at 300 K compared with bandgaps of other PV materials with unconcentrated ($C = 1$) and high concentration ($C = 1000$) sunlight.

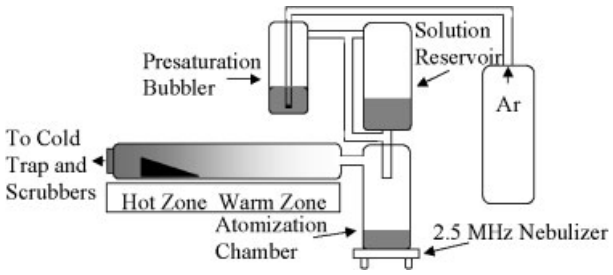

Figure 3. Schematic for spray CVD apparatus.

can be tuned from 1.0 to 2.4 eV, thus permitting fabrication of high, or graded bandgaps.[6]

One of the key technical issues outlined in the 2001 PV Industry Roadmap is the need to develop low-cost, high-throughput manufacturing for high-efficiency thin-film solar cells. Thus, a key step for device fabrication for thin-film solar cells is the deposition onto flexible, lightweight substrates such as polyimides. Current methods for depositing ternary crystallite compounds include co-evaporation of elements[7–9] or alloys,[10] electrodeposition,[11] reactive-sintering,[12] and flash evaporation,[13] which are often followed by toxic sulfurization/selenization steps, at elevated temperatures. Furthermore, under these conditions, loss of volatile indium/galium chalcogenides is common.[7,14] The high temperature requirements make this protocol incompatible with all presently known flexible polyimides, or other polymer substrates. In addition, the use of toxic reagents is a limiting factor. The use of multi-source inorganic/organometallic precursors in a chemical vapor deposition (CVD)-type process is more appealing owing to milder process parameters. However, stoichiometric control of deposited films can be difficult to achieve, and film contamination has been reported.[15,16] A novel alternative approach is the use of ternary single-source precursors (SSPs). They have the I–III–VI_2 stoichiometry 'built in' and are suitable for low-temperature deposition (Plate 1). Although a rich and diverse array of binary SSPs[17–21] are known, characterized, reviewed, and tested, the number of known ternary SSPs is limited, as is their use in deposition processes.[17] Hence, it is the goal of this review to highlight recent advances carried out at our laboratories and by other groups, summarizing a highly promising technique for thin-film growth, via molecular design of SSPs for use in a CVD process.

Spray CVD

Spray CVD has become an increasingly used technique. In this process, a room-temperature precursor solution is ultrasonically nebulized, and is swept into a two-zone, hot-wall reactor (Fig. 3). The carrier-solvent is evaporated in the warm zone, and the gaseous precursors are decomposed in the hot zone, where film growth occurs as in conventional CVD. Spray CVD maintains the most desirable features of Metalorganic CVD (MOCVD) and spray pyrolysis, such as film growth in inert atmospheres, large-area deposition, laminar flow over the substrate, and a low-temperature solution reservoir, while avoiding the major difficulties of each.[22,23] It minimizes the high volatility and temperature requirements for the precursor, which are essential in MOCVD, by delivering the precursor to the furnace as an aerosol propelled by a fast-flowing carrier gas from a low-temperature precursor reservoir analogous to that employed in spray pyrolysis. The latter feature is an important benefit that can prevent premature precursor decomposition when using thermally labile precursors.

PREVIOUS WORK

In early studies Nomura *et al.*[24] reported that an equimolar mixture of [^{i}Bu_2InSPr] and [$Cu(S_2CNBu_2)_2$] decomposed to afford $CuInS_2$ powders. On this basis, solution pyrolysis of this mixture dissolved in *p*-xylene was used to deposit thin-film $CuInS_2$ at 350 °C onto glass substrates. Film composition was determined by X-ray diffraction (XRD), which showed broad peaks. XRD revealed that the ratios of In/Cu and S/Cu decreased with temperature, and that a second phase was present for films deposited at 350 °C. Grain size was estimated to be in the range of 50–100 nm as determined by scanning electron microscopy (SEM). It was later realized that the equimolar reaction mixture of [^{i}Bu_2InSPr] and [$Cu(S_2CNBu_2)_2$] (as used in solution pyrolysis) afforded the SSP [$Bu_2In(S^iPr)Cu(S_2CN^iPr_2$] before decomposing to the

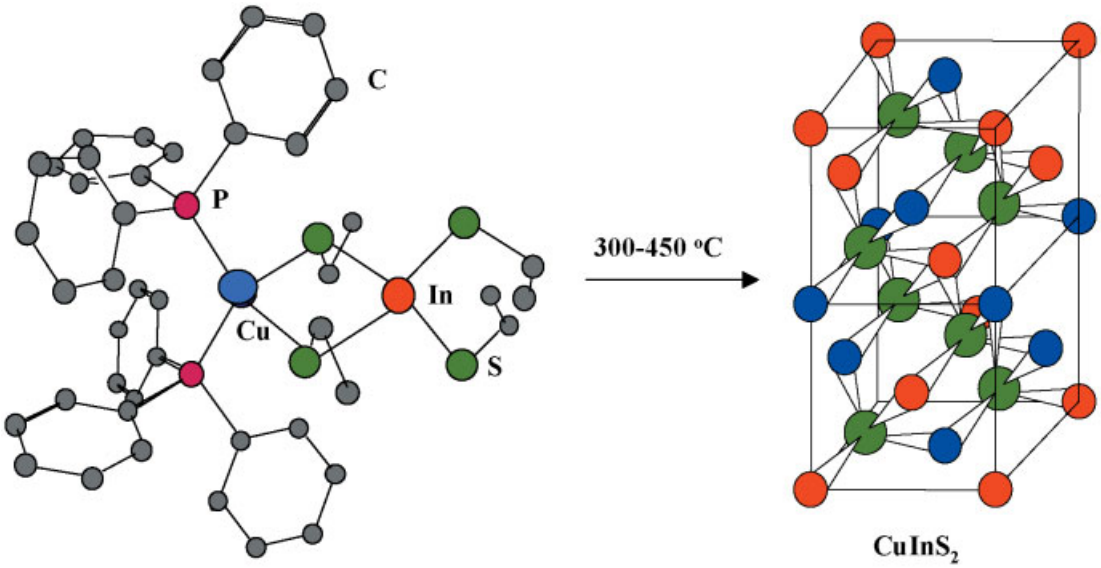

Plate 1. Pyrolysis of SSP $[\{PPh_3\}_2Cu(SEt)_2In(SEt)_2]$,to afford the semiconductor $CuInS_2$.

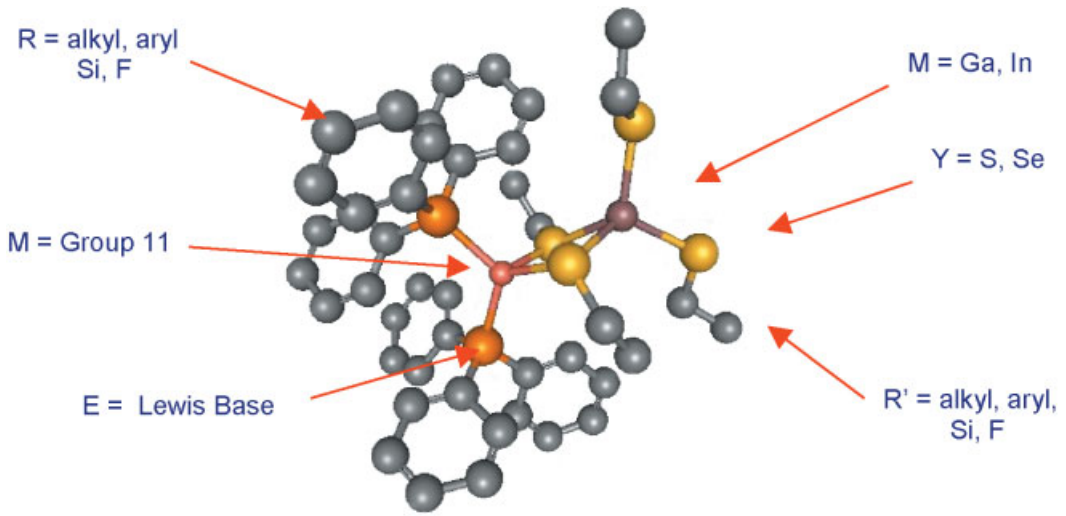

Plate 2. Single-crystal structure of $[\{PPh_3\}_2Cu(SEt)_2In(SEt)_2]$,[28] indicating '*tunable*' sites.

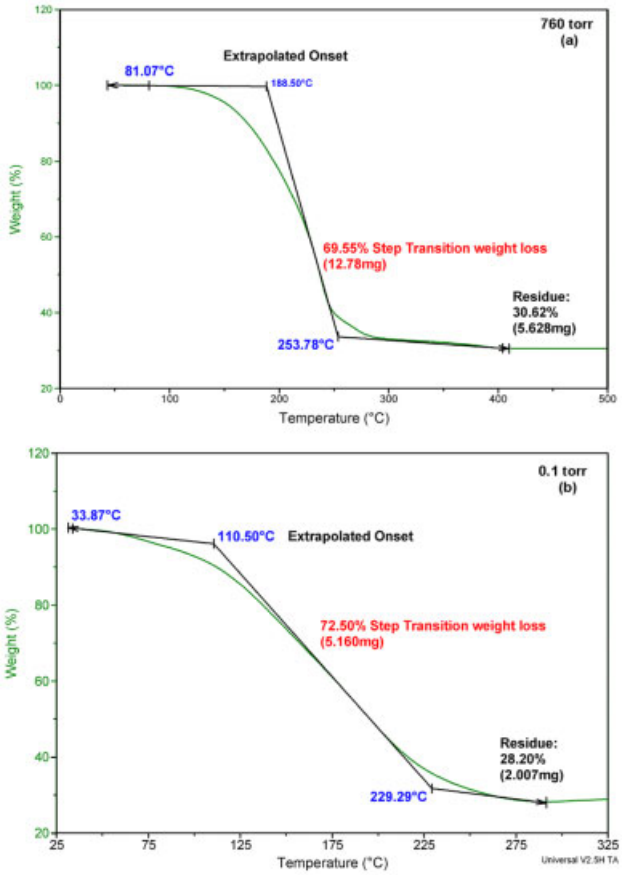

Plate 3. TGA profiles for $[\{P(^{n}Bu)_3\}_2Cu(SEt)_2In(SEt)_2]$ (**7**).

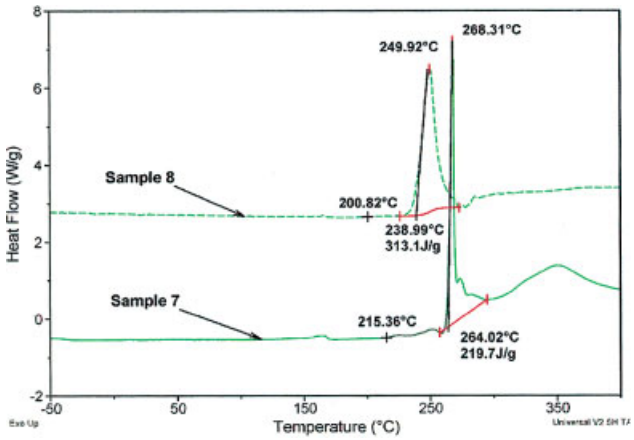

Plate 4. Low-temperature DSC for $[\{P(^{n}Bu)_3\}_2Cu(SEt)_2In(SEt)_2]$ (**7**) and $[\{P(^{n}Bu)_3\}_2Cu(S^{n}Pr)_2In(S^{n}Pr)_2]$ (**8**).

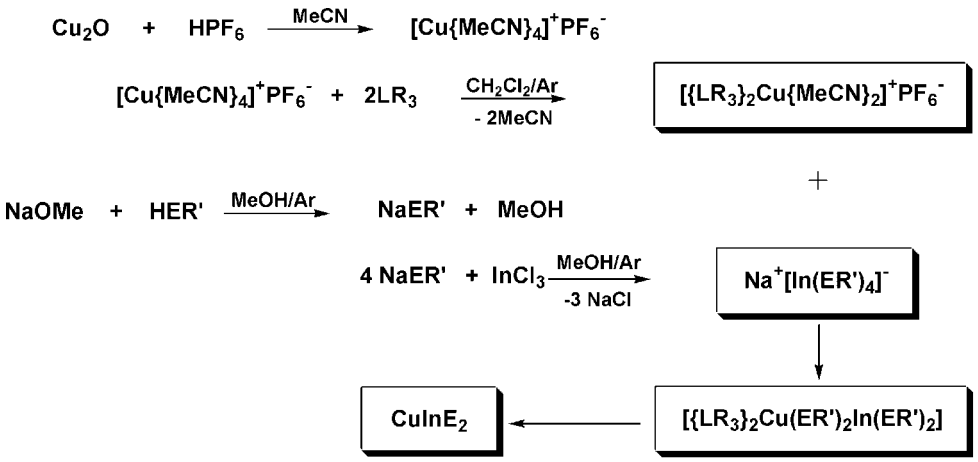

Scheme 1. Synthesis of ternary SSPs.

chalcopyrite matrix.[25] Analytical and spectral data confirmed that the mixture of [^{i}Bu$_2$InSPr] and [Cu(S$_2$CNBu$_2$)$_2$] yielded an SSP. A number of analogous ternary CIS precursors were also synthesized by the reaction of alkyl indium thiolates with copper dithiocarbamates:[26]

$$2\mathrm{R\,In(SPr)_2} + 2\mathrm{Cu(S_2CNR'_2)_2} \rightarrow 2[\mathrm{R\,In(SPr)_2Cu(S_2CNR'_2)}] + (\mathrm{R'_2NCS_2})_2 \quad (1)$$

$$\mathrm{R} = \mathrm{Bu}, {}^{i}\mathrm{Bu}, {}^{s}\mathrm{Bu}; \mathrm{R'} = \mathrm{Et}, \mathrm{Bu}$$

However, only [Bu$_2$In(S^{i}Pr)Cu(S$_2$CN^{i}Pr$_2$] was successfully implemented for depositing pure CuInS$_2$ by low-pressure MOCVD. In the case of [BuIn(S^{i}Pr)$_2$Cu(S$_2$CNR′$_2$)], tetragonal CuIn$_5$S$_8$ was deposited:[27]

$$[\mathrm{Bu\,In(SPr)_2Cu(S_2CNR'_2)}] \xrightarrow{400^{\circ}\mathrm{C}/0.6\mathrm{Torr}} \mathrm{Cu_5\,In\,S_8} \quad (2)$$

$$\mathrm{R} = \mathrm{Bu}, {}^{i}\mathrm{Bu}, {}^{s}\mathrm{Bu}; \mathrm{R'} = \mathrm{Et}, \mathrm{Bu}$$

In early 1990 Kanatzidis and coworkers[28] reported the preparation of hetero-binuclear complexes consisting of tetrahedrally arranged copper and indium centers, with two bridging thiolato and selenolato groups:

$$[\{\mathrm{Ph_3P}\}_2\mathrm{Cu(MeCN)_2}]^{+} + [\mathrm{In(ER)_4}]^{-} \xrightarrow{\mathrm{MeOH}} [\{\mathrm{Ph_3P}\}_2\mathrm{Cu}(\mu\text{-}\mathrm{ER})_2\mathrm{In(ER)_2}] + 2\mathrm{MeCN} \quad (3)$$

Pyrolysis studies undertaken revealed that the selenium derivative could be converted into CuInSe$_2$ at 400–450 °C at 0.01 mmHg [Eqn. (4)], but none of the precursors had been evaluated in a thin-film deposition study:

$$[\{\mathrm{Ph_3P}\}_2\mathrm{Cu}(\mu\text{-}\mathrm{SeEt})_2\mathrm{In(SEt)_2}] \xrightarrow{400\text{–}350^{\circ}\mathrm{C}/0.01\ \mathrm{mmHg}} \mathrm{CuInSe_2} + 2\mathrm{PPh_3} + 2\mathrm{EtSeEt} \quad (4)$$

In continuing work, Hepp and coworkers[29–31] were able to demonstrate that [{PPh$_3$}$_2$Cu(SEt)$_2$In(SEt)$_2$] could be utilized in a spray CVD process for depositing thin-film CuInS$_2$ below 400 °C. Thin films where deposited using a dual solvent system of toluene and dichloromethane (CH_2Cl_2) as the carrier solvent. Single-phase (112)-oriented CuInS$_2$ thin films were successfully deposited at a range of temperatures from 300 to 400 °C, while at elevated temperatures (>500 °C) CuIn$_5$S$_8$ phase thin films could be deposited. Rutherford backscattering (RBS), energy dispersive spectroscopy (EDS), and X-ray photoelectron spectroscopy (XPS) analysis showed that the films were free from any detectable impurities and highly crystalline, thus concluding that the precursor decomposes cleanly. During the course of the study, the morphology of the deposited thin films was found to be temperature-, and carrier-solvent-dependent. Films deposited at 300 and 350 °C yielded grain size of 400–800 nm, with smaller finer particles of 50–200 nm resident on top. At the higher deposition temperature of 400 °C the films consisted of more angular and uniform grain size of approximately 200–400 nm. Photoluminescence (PL) data and optical transmission measurements confirmed the deposited CuInS$_2$ thin films were direct bandgap semiconductors.

In the course of our investigations on improved SSP for the spray CVD of chalcopyrite thin films of the ternary semiconductor CIS, we have continued to expand the molecular design of SSPs based on the [{LR$_3$}$_2$Cu(ER′)$_2$M(ER′)$_2$] architecture.[28] This was done primarily because of the limited prior preparation and use of these complexes for spray CVD. Furthermore, the number of 'tunable' sites within the complex allows for their utility in preparing a number of ternary chalcopyrites of varying composition, in addition to being able to engineer the SSP to match a given spray CVD process (Plate 2).

Table 1. Thermal data for ternary SSPs

	TGA			DSC	
Single Source Precursors	Extrap. onset (°C)	MRW (°C)	Residue (%)	M.P. (°C)	Decomp. (°C)
1 $[\{PPh_3\}_2Cu(SEt)_2In(SEt)_2]$	236	269	25	122	266
2 $[\{AsPh_3\}_2Cu(SEt)_2In(SEt)_2]$	205	233	18	47	276
3 $[\{SbPh_3\}_2Cu(SEt)_2In(SEt)_2]$	212	239	26	45	271
4 $[\{PPh_3\}_2Cu(S^iPr)_2In(S^iPr)_2]$	215	254	29	163	260
5 $[\{PPh_3\}_2Cu(SPh)_2In(SPh)_2]$	261	325	22	117	280
6 $[\{PPh_3\}_2Cu(SePh)_2In(SePh)_2]$	223	253	22	53	219
7 $[\{P(^nBu)_3\}_2Cu(SEt)_2In(SEt)_2]$	189	238	31	–	264
8 $[\{P(^nBu)_3\}_2Cu(S^nPr)_2In(S^nPr)_2]$	171	225	29	–	239
9 $[\{PPh_3\}_2CuGa(SEt)_x]$[a]	[b]	310	25	[b]	[b]

[a] Structure not eludicated ($x = 3$, or 4).
[b] Not recorded.

CHEMICAL SYNTHESIS

The SSPs are prepared by the reaction of a stabilized copper(I) cation, with an indium(III), or gallium(III) chalcogenide anion prepared *in situ* by reaction of the conjugate acid of the thiol or senenol with NaOEt in methanol[32,33] (Scheme 1). The versatility of this synthetic pathway is illustrated by ability to modulate the physical properties of the precursor and composition at any of the intermediate synthetic steps by:

- adjusting the Lewis acid–base interaction (L→M, M is a group 11 metal)
- adjusting the accessibility of the lone pair of electrons on the neutral donor ligand by variation of R
- adjusting the bond strength between the chalcogenide with either indium/galium or copper metal centers
- the ability to prepare analogs of group 16 (sulfur, selenium, tellurium)
- the ability to prepare either indium or gallium derivatives.

The Lewis acid–base interaction is a valuable component to the overall stability of the molecule, given that the ability of the Lewis base to dissociate from the cation at lower energies is pertinent to the degradation of the precursor at reduced temperatures. Hence, the Drago–Wayland approximation[34] can be used for ternary SSP design, to estimate quantitatively the strength of the Lewis acid–base interaction between the copper center and the neutral donor. The cleavage of chalcogenide–R′ bond also plays an important role, since this allows the chalcogenide to be released for incorporation into the ternary chalcopyrite matrix. Hence, the use of a sterically demanding R′ group with good 'leaving ability' would promote the facile release of the chalcogenide.

CHARACTERIZATION

Initial studies focused on basic modification of the SSPs, and their influence on precursor stability. Multinuclear NMR data demonstrated that the precursors were free from any starting reagents. Thermogravimetric analysis (TGA) was performed at ambient pressure in platinum pans on samples of the precursors, heated at a rate of 10 °C min^{-1} under a dinitrogen atmosphere. Weight loss was associated with decomposition of the complexes. Calculation of the derivative maximum rate of weight loss (%/°C), listed as MRW (temperature) in Table 1, shows a range from a low of 225 °C for **8** to a high of 325 °C for **5**. Calculation of the precursor efficiency to afford CIS/Se as the final product, based on the residual material from the TGA experiments, found the samples to be within 5% (Plate 3a).

A further example of the flexibility of the $[\{LR_3\}_2Cu(ER')_2M(ER')_2]$ architecture to direct adjustment of these precursors are the SSPs **7** and **8**, which represent the first liquid SSPs for the decomposition to $CuInS_2$[32]. Low-temperature differential scanning calorimetry (DSC) was used to investigate the liquid phase for **7** and **8**. In separate studies, samples **7** and **8** were subjected to both quench cooling and slow controlled cooling before being heated at 10 and 5 °C min^{-1}; the higher heating rates were chosen since this is preferable to enhance resolution for the observation of a finite onset point assignable to melting, see Ref. 35. In low-temperature DSC experiments using controlled and quench cooling, both samples **7** and **8** were found not to show an endotherm assignable to a melting phase transition, thus confirming their liquid phase at ambient temperatures (Plate 4).

Examination of the other phase transitions reveals that the main exothermic events for **7** and **8** begin with extrapolated onset temperatures of 264 °C and 239 °C respectively, which represent the decomposition of the samples. The lower decomposition temperature of **8** can be explained, since an increase in chain length and/or steric 'bulk' of the alkyl groups is known to decrease the stability of a complex.[17] In addition, preliminary vacuum-TGA studies for the

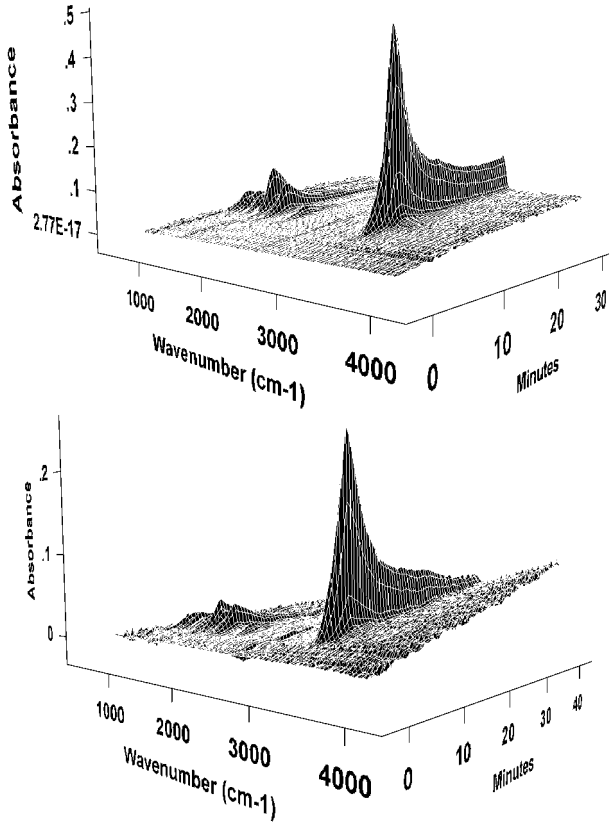

Figure 4. EGA-FTIR spectra for $[\{P(n\text{-}Bu)_3\}_2Cu(SEt)_2In(SEt)_2]$ (**7**) and $[\{P(^nBu)_3\}_2Cu(S^nPr)_2In(S^nPr)_2]$ (**8**).

'smoothed' profile for SSP **7** show that the extrapolated onset can be lowered by approximately 80 °C, thus lowering the degradation temperature window and making these precursors highly suitable for use in low-temperature/pressure spray CVD on space-qualified substrates such as Kapton™ (Plate 3b). Remarkably, both liquid precursors show excellent solubility in both polar and non-polar solvents, which can be attributed to their ionic structure and the non-polar alkyl groups resident on the tertiary phosphine.

The ability of the new precursors to decompose thermally to yield single-phase CIS was investigated by powder XRD analysis and EDS on the non-volatile solids from the TGA experiments of selective compounds. Furthermore, using TGA-evolved gas analysis (EGA), the volatile components from the degradation of the SSPs could be analyzed via real-time FTIR and mass spectroscopy, thus providing information for the decomposition mechanism.[36] The real-time FTIR spectram for **7** and **8** show absorptions at approximately 3000, 1460, 1390, 1300, and 1250 cm^{-1} (Fig. 4).

Correlation with the EGA-mass spectra allows for the assignment to the initial loss of diethyl sulfide, as supported by the library fit and from the assignment of the fragment and parent ions ($m/z = 90$) (Fig. 5a). After approximately

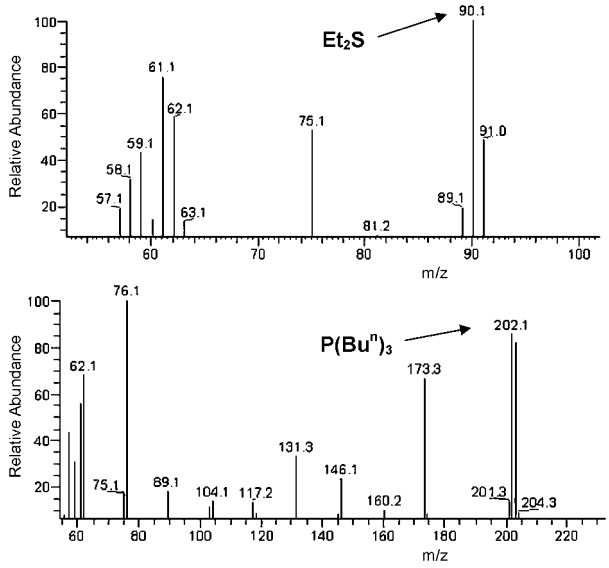

Figure 5. EGA-MS (EI) data for $[\{P(^nBu)_3\}_2Cu(SEt)_2In(SEt)_2]$ (**7**).

15 min, EGA mass spectroscopy shows the absence of peaks assignable to Et_2S and the occurrence of fragment ions with $m/z > 90$ with an intense peak at $m/z = 202$. These can be assigned to the successive loss of PBu_3 on the basis of its library fit of 92% and assignment of the fragment ions (Fig. 5b). Thus, the use of TGA-EGA provides conclusive evidence for the mechanism of decomposition for the SSPs to occur via the initial loss of a chalcogenide moiety, followed by loss of the neutral donor ligand.

Comparison of the XRD spectra for the non-volatile material produced from the pyrolysis of **7** with the JCPDS reference patterns for $CuInS_2$ (27-0159) confirmed it to be single-phase $CuInS_2$ (Fig. 6). Examination of the EDS spectra for the same samples shows predominant emissions due to

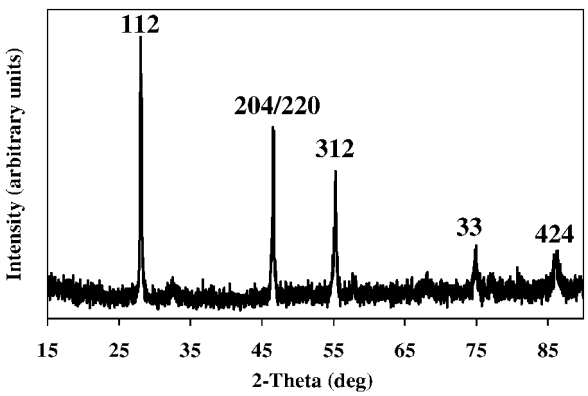

Figure 6. XRD powder diffraction for non-volatile residue from pyrolysis of $[\{P(^nBu)_3\}_2Cu(SEt)_2In(SEt)_2]$, (Cu Kα, 1.541 Å).

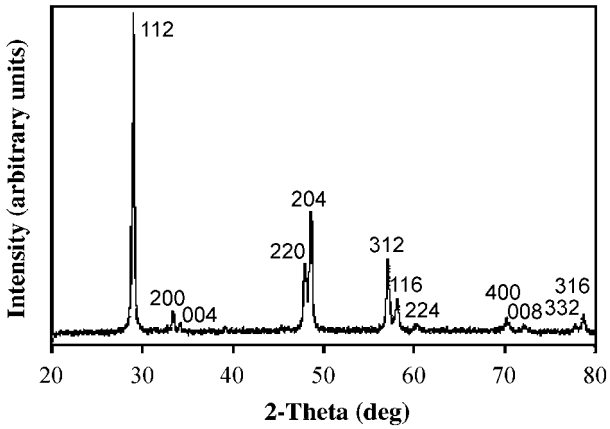

Figure 7. XRD pattern of non-volatile solid obtained from bulk pyrolysis of $[(Ph_3P)_2CuGa(SEt)_x]$(**9**; 600 °C, 300 min). All reflections correspond to gallite $CuGaS_2$ (JCPDS # 25-0279).

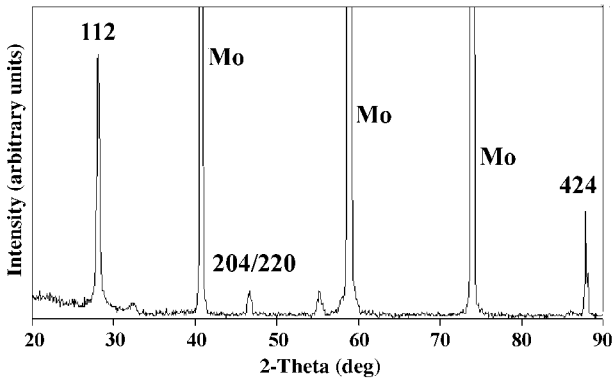

Figure 8. X-ray powder diffraction spectra of a $CuInS_2$ thin film on Mo using SSP **7**.

copper, indium, and sulfur edges, with the respective approximate percentage atomic compositions of 27%, 23%, and 50% for **7** and 28%, 23%, and 49% for **8**, thus supporting the formation of $CuInS_2$.

The preparation of the first SSP to the semiconductor $CuGaS_2$ was also investigated.[33] Although the molecular structure for SSP **9** was not fully characterized, its suitability to afford bulk and thin-film $CuGaS_2$ was studied by TGA (Table 1) and XRD. In addition, the optical properties of the deposited thin films were also investigated. Powder XRD analysis on the non-volatile product from bulk pyrolysis (N_2, 600 °C) confirmed the collected material to be single-phase (112)-oriented $CuGaS_2$ (Fig. 7), having an average coherence length of 28 nm.

THIN-FILM STUDY

Well-adhering films of $CuInS_2$ were deposited onto a molybdenum substrate by spray CVD at 390 °C using $[\{PBu_3\}_2Cu(SEt)_2In(SEt)_2]$; these were dark blue–black, due to variation in film thickness. As deposited, the $CuInS_2$ film is highly (112)-oriented (Fig. 8); this is ideal, since the preferred orientation for CIS films used in PV devices is (112), as these films have a low series resistance.[37]

Table 2. Atomic composition of CIS thin film deposited using SSP **7**

	Atomic % (±3%)		
	Front 1	Front 2	Back
Cu	50	51	50
In	50	49	50

Measurements of the EDS emission were limited to copper and indium edges, since the EDS emissions for sulfur and molybdenum overlapped. SEM–EDS data on a number of regions on the thin film gave atomic percentages representative of $CuInS_2$ (Table 2); and no evidence of phosphorus or

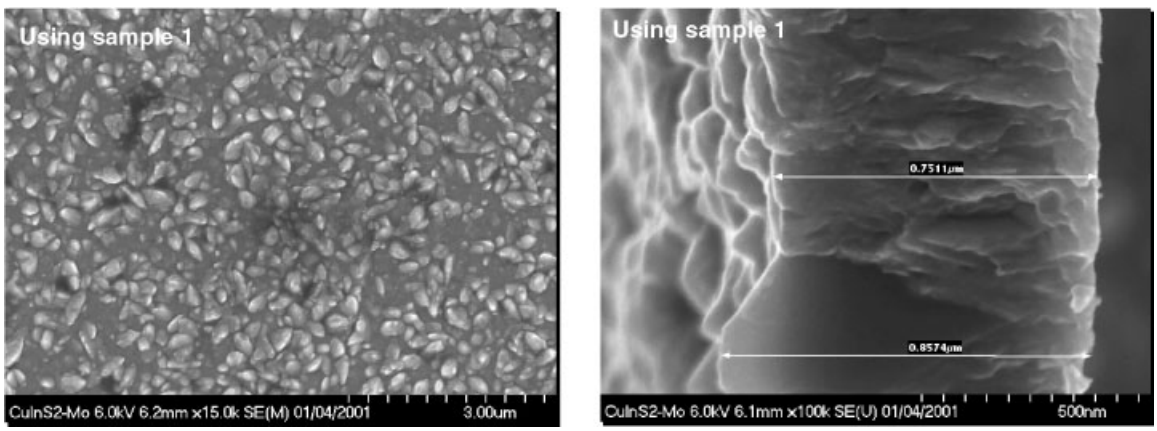

Figure 9. SEM of deposited CIS film using $[\{P(PPh)_3\}_2Cu(SEt)_2In(SEt)_2]$ (**1**).

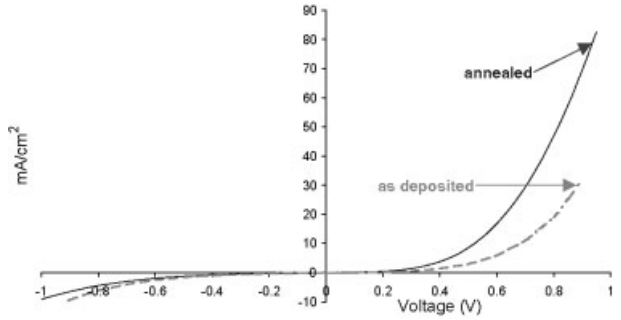

Figure 10. Current density versus voltage plot of Schottky barrier made from evaporated aluminum on $CuInS_2$ on molybdenum foil using SSP **1**.

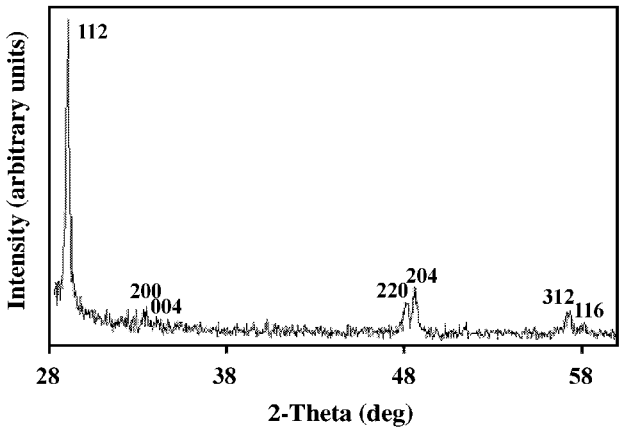

Figure 11. XRD pattern of spray-CVD-grown $CuGaS_2$ film on Si(111), using SSP **9**. Reflections correspond to those reported for gallite in JCPDS reference # 25-0279.

carbon contamination could be detected, verifying that the precursor decomposes cleanly, as evidenced in EGA-TGA studies.

Unfortunately, owing to the limited quantities of the liquid precursor for thin-film deposition, no electronic properties of the film could be performed, since film thickness was insufficient for device fabrication. However, the electrical properties of deposited films (Fig. 9) using SSP **1** have been shown to make excellent Schottky barriers.[35] The electrical properties of the deposited films were evaluated by current versus voltage (I–V) measurements, recorded for the thin films using thermally evaporated aluminum contacts ($10\ \mu m^2$) to make Schottky barrier diodes (Fig. 10).

The Schottky barriers were excellent diodes on films annealed at 600 °C, with 'turn on' voltages of 0.6–0.8 V, and minimal reverse bias leakage. However, many of the contacts on the as-deposited films gave large reverse bias currents and nearly ohmic responses. This behavior is indicative of degeneracy of the semiconductor due to a high carrier density resulting from native defects. The improvement in the diode behavior of the annealed films is attributed to enhanced crystallinity and reduction of defects.

Spray CVD deposition studies utilizing the new galium SSP **9**, in a toluene–CH_2Br_2 solution (0.01 M: 86 vol% toluene; 1.3 mmol; SSP **9**) afforded well-adhered dense thin film (450 ± 5 °C, 4.0 l min^{-1}). The films were visually smooth and optically transparent, exhibiting a pink and green surface tint. XRD analysis confirmed the film to be highly (112) oriented, tetragonal single-phase $CuGaS_2$ (Fig. 11).

The (220)/(204) reflections and the (312)/(116) reflections were split consistent with the tetragonal distortion of the crystal lattice[39] (Fig. 11). Lattice parameters a and c were calculated from X-ray d spacings according to Eqn. (5), where h, k, and l refer to the Miller indices of individual reflections.[40]

$$\frac{1}{d^2} = \frac{h^2 + k^2}{a^2} + \frac{l^2}{c^2} \tag{5}$$

The d spacing of the (220) reflection was used to calculate a, and the d spacing of the (112) reflection was used with the calculated lattice parameter a to determine c. The lattice parameters, c/a ratio and the distortion parameter x (where $x = 2 - c/a$, given that a hypothetical $c/a = 2$ would result in the *absence* of any tetragonal distortion) are presented in Table 3. Comparison of the data collected from the $CuGaS_2$ thin film shows they are in good agreement with the JCPDS reference values for single-crystal $CuGaS_2$ and with those reported in literature.[41]

SEM images reveal that the films are dense, with an average grain size of 410 nm, and oriented predominantly in a vertical manner (Fig. 12c and d). The surface microstructure consisted of faceted grains, many of which exhibited a trigonal shape (Fig. 12a and b), which occurs as a result of close-packed intersecting (112) faces of the chalcopyrite lattice. These are the lowest surface-energy faces and typically control chalcopyrite morphology.[21,42] The grain

Table 3. Comparison of thin-film and single-crystal $CuGaS_2$ lattice parameters, a and c, c/a, and the distortion parameter x

a (Å)	c (Å)	c/a	x	Thin-film fabrication method
5.353	10.495	1.9606	0.0394	Spray-CVD-deposited film
5.35	10.48	1.959	0.0410	Evaporated film[41]
5.351	10.484	1.9593	0.0407	JCPDS card 25-0297: single crystal prepared from the elements

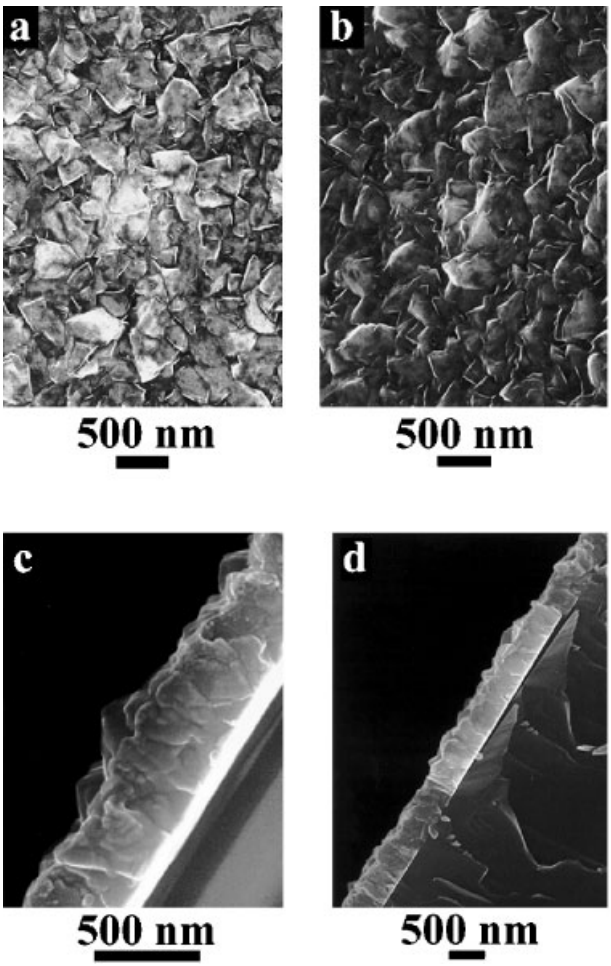

Figure 12. SEM images of $CuGaS_2$ films deposited by spray CVD: (a) surface view showing crystalline, faceted, approximately equiaxed grains; (b) surface view; 30° tilt showing triangular shape of many of the grains characteristic of (112)-oriented crystals; (c) and (d) edge views showing roughly columnar crystal-growth pattern and dense nature of the film. Triangular grains protruding from the film surface are visible in (c).

sizes observed by SEM are considerably larger than the average coherence lengths calculated from X-ray line broadening, which could have been reduced by a high defect density in the grains or by strain in the film.

Sheet resistivity for the $CuGaS_2$ thin-film samples was determined using the four-point probe method ($\rho = R_s t$, where t is the film thickness).[43] Sheet resistance was calculated from current–voltage data (Fig. 13) by $R_s = K_p V/I$, where K_p is a constant (for a probe of the type used here, and for a sample with planar dimensions that can be considered infinite relative to the probe spacing, $K_p = \pi/\ln 2$). The resistivity determined for the film deposited at 450 °C on fused silica was found to be 15.6(4) Ω cm, which is an order of magnitude greater than the resistivity of 1.0 Ω cm

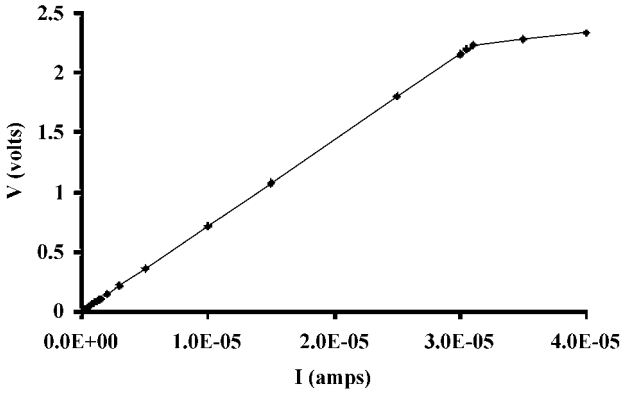

Figure 13. *V–I* curve for $CuGaS_2$ thin film. The linear region below 3.0×10^{-5} was used to calculate sheet resistance.

obtained from melt-grown single-crystal $CuGaS_2$ (S-annealed).[43]

The optical bandgap of the films was determined from optical transmittance data, which showed the film to absorb incident light below 480 nm (Fig. 14a). Transmittance was observed to change most dramatically in the region from 480

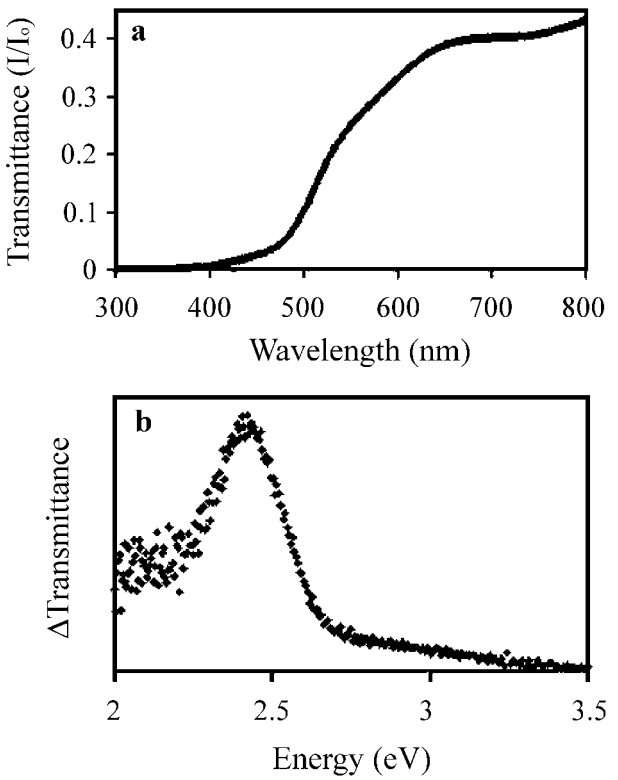

Figure 14. (a) Transmittance versus wavelength for $CuGaS_2$ thin film; (I, transmitted power; I_o, incident power. (b) Plot of the derivative of the transmission data versus energy.

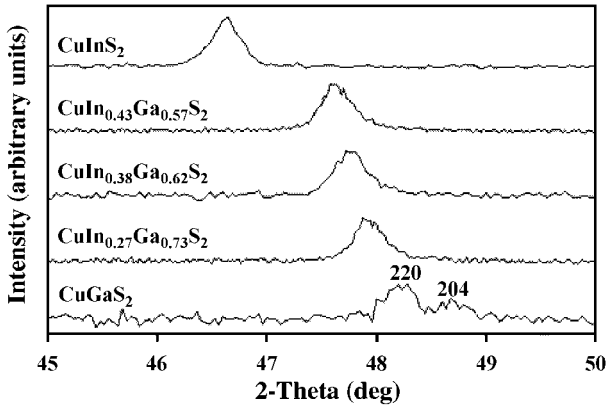

Figure 15. XRD spectra highlighting the (220)/(204) reflections of a $CuGaS_2$ film (bottom, T_s = 450 °C), a $CuInS_2$ film (top; T_s = 400 °C), and alloy films having In_xGa_y contents in the range $In_{0.43}Ga_{0.57}$ to $In_{0.27}Ga_{0.73}$. All films were deposited on fused silica.

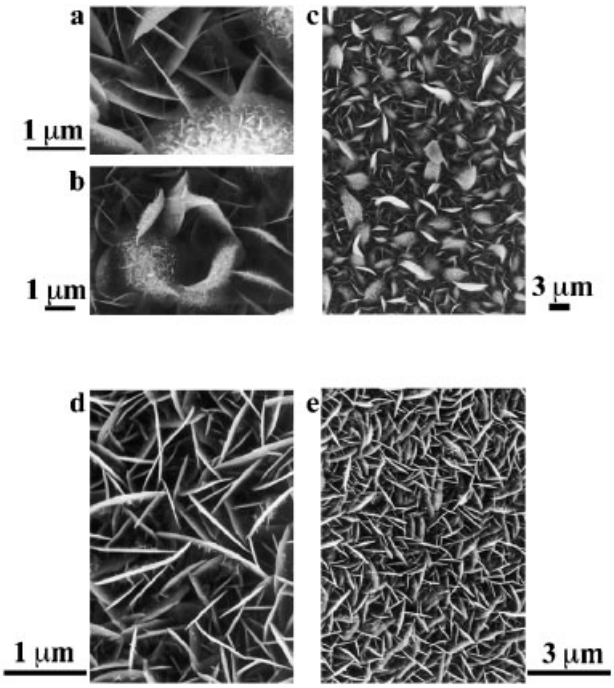

Figure 16. SEM images of the alloy film showing the variation in microstructure with composition: (a)–(c) film deposited in the first centimeter: $CuIn_{0.43}Ga_{0.57}S_2$; (d) and (e) film deposited in the last centimeter: $CuIn_{0.27}Ga_{0.73}S_2$.

to 540 nm, which is the region of the direct absorption edge. Calculation of the derivative for the transmission curve provided a more precise method to determine the bandgap within this region,[44] yielding a maximum at 2.42 eV (Fig. 14b). This value is in very good accord with the known direct bandgap of $CuGaS_2$ reported in the literature, E_g = 2.43 eV.[45]

Initial studies using the two analogous galium and indium SSP, for fabrication of an alloy film, $Cu(In:Ga)S_2$, in a dual-source spray CVD were also investigated. A film was deposited from a mixed toluene solution of $[\{Ph_3P\}_2Cu(SEt)_2In(SEt)_2]$ (**1**; 0.0075 M) and the galium analog **9** (0.0025 M).[33] Although a thin film was deposited, the composition and microstructure varied along the length of the thin film. XRD reflections representing the (112) planes were broad and complicated by the presence of an unidentified reflection in that region. The (220)/(204) planes were represented by a single, unresolved reflection that yielded an average grain size of ~40 nm. The relative contributions of galium and indium to the multinary structure were determined by comparing the 2θ values for this reflection in the multinary pattern with those in the patterns of the ternary end-members, $CuInS_2$ and $CuGaS_2$ (Fig. 15). The composition of each metal was assumed to vary linearly with 2θ from 100% indium to 100% galium based on Vegard's law. The tetragonal splitting was neglected in the $CuGaS_2$ pattern by averaging the 2θ values for the (220) and the (204) reflections.

The atomic percentage of galium in the film was found to increase along this length from the front to rear of the film. The film deposited in the first centimeter had a composition of $CuIn_{0.43}Ga_{0.57}S_2$; in the middle the composition was $CuIn_{0.38}Ga_{0.62}S_2$; that deposited in the last centimeter had the highest contribution of galium $CuIn_{0.27}Ga_{0.73}S_2$. A uniform composition over large areas was, therefore, not achieved, and, interestingly, none of the compositions were close to the expected $In_{0.75}Ga_{0.25}$ ratio in accord with the precursor molar ratio. SEM images of the films (Fig. 16) revealed that the microstructure was similar to that observed for $CuInS_2$ deposited at 450 °C.[30] The variation in film composition is understandable, since the two precursor thermal decomposition profiles are unalike. Therefore, using two SSPs with matching thermal profiles may provide an effective means for depositing multi-ternary films.

SUMMARY AND OUTLOOK

The versatility of the $[\{LR_3\}_2Cu(ER')_2M(ER')_2]$ architecture is clearly demonstrated by the preparation of SSPs to multi-ternary semiconductors. Thermal analysis data substantiates that steric and electronic molecular modification, on either the neutral donor or the chalcogenide, permit directed adjustment of the solid-state phase and stability of the precursors. EGA confirms that the mechanism of decomposition for the SSPs proceeds 'cleanly' by the loss of the chalcogenide moiety, followed by loss of the neutral donor. Spray CVD using SSPs is a mild, simple, clean, and scalable technique for depositing $CuInE_2$ or $CuGaE_2$ (E = S, Se) thin films on flexible polymer substrates at reduced temperatures. Although tests for the deposition of the wide bandgap alloy $Cu(Ga:In)S_2$ led to a non-homogeneous film composi-

tion, it is evident that, with the use of two SSPs with similar thermal profiles, consistent film stoichiometry may be achieved.

Clearly, the full potential of CIS PV devices has not been fully exploited, since the combination of group I–III–VI_2 elements can result in a variety of end products. Therefore, correlations need to be made that can associate device processing, fabrication, film composition, etc. to cell band-gap and efficiency. Spray CVD in conjunction with SSP design provides a proof-of-concept for a manufacturable process. The following further investigation needs to be undertaken. (1) *Precursor design*: development of more volatile/thermally labile systems. This can be achieved by the incorporation of fluorinated or silylated functional groups. Importantly, becaue of the well-known tendency of flourine to react with silyl moieties, incorporation of both elements in the molecule can serve not only to increase volatility, but can also provide a 'self-cleaning' mechanism should the precursor decompose by an undesired pathway. (2) *Processing parameters*: spray CVD has a number of tunable variables, such as droplet size, flow-rate, concentration, and solvent polarity, that are advantageous for achieving the desired film characteristics. Thus, an in-depth study needs to address these parameters to film composition. (3) *Device fabrication*: working devices from deposited films need to be tested to aid SSP design and spray CVD process parameters. The work reported here on the molecular design of SSPs for their use in a spray CVD process, although still in its infancy, undoubtedly shows it to be a mass production, cost-effective method for fabricating commercial thin-film PV devices.

Acknowledgements

We would like to acknowledge the collaboration of scientists and researchers from government, industry and university laboratories who have helped in the development of this project. In addition, we gratefully acknowledge the National Aeronautics and Space Administration (NASA) for financial support with cooperative agreements NCC3-817, NCC3-563, and NCC3-734.

REFERENCES

1. Contreras M, Egaas B, Ramanathan K, Hiltner J, Swartlander A, Hasoon F and Noufi R. *Prog. Photovolt. Res. Appl.* 1999; **7**: 311.
2. Hoffman D, Kerslake T, Hepp AF and Raffaelle R. Thin-film solar array Earth-orbit mission applicability assessment. In *XVII Space Photovoltaic Research and Technology Conference* 2001.
3. Bailey SG and Flood DJ. *Prog. Photovolt. Res. Appl.* 1998; **6**: 1.
4. Schock HW and Noufi R. *Prog. Photovolt. Res. Appl.* 2000; **8**: 151.
5. Schock HW, Bogus K. Development of CIS solar cells for space applications. In *Proceedings 2nd World Conference on Photovoltaic Energy*, Schmid J, Ossenbrink HA, Helm P, Ehmann H and Dunlop ED (eds). EC Joint Research Center, Luxembourg, 1998; 3586.
6. Tarrant D and Ermer J. I–III–VI_2 multinary solar cells based on $CuInSe_2$. In *Proceedings 23rd IEEE Photovoltaic Specialist Conference*, Louisville KY. IEEE: New York, 1993; 372–378.
7. Basol BM, Kapur VK, Halani A, Leidholm C, Sharp J, Sites JR, Swartzlander A, Matson R and Ullal H. *J. Vac. Sci. Technol. A* 1996; **14**: 2251.
8. Probst V, Stetter W, Riedl W, Vogt H, Wendl M, Calwer H, Zweigart S, Ufert K, Freienstein B, Cerva H and Karg FH. *Thin Solid Films* 2001; **387**: 262.
9. Dimmler B and Schock HW. *Prog. Photovolt. Res. Appl.* 1998; **6**: 193.
10. Park SC, Lee DY, Ahn BT, Yoon KH and Song J. *Sol. Energy Mater. Sol. Cells* 2001; **69**: 99.
11. Guillen C and Herrero J. *Thin Solid Films* 2001; **387**: 57.
12. Eberspacher C, Fredric K, Pauls K and Serra J. *Thin Solid Films* 2001; **387**: 18.
13. Klenk M, Schenker O, Alberts V and Bucher E. *Thin Solid Films* 2001; **387**: 47.
14. Dzionk C, Metzner H, Hessler S and Mahnke HE. *Thin Solid Films* 1997; **299**: 38.
15. Krunks M, Mikli V, Bijakina O, Hebane H, Mere A, Varema T and Mellikov E. *Thin Solid Films* 2000; **361–362**: 61.
16. Artaud MC, Ouchen F, Martin L and Duchemin S. *Thin Solid Films* 1998; **324**: 115.
17. Jones AC and O'Brien P. *CVD of Compound Semiconductors: Precursors Synthesis, Development & Application*. VCH Press: 1997.
18. Rees WS. Introduction. In *CVD of Nonmetals*, Rees WS (ed.). VCH Press: 1996, 1–35.
19. Keys A, Barbarich T, Bott SG and Barron AR. *J. Chem. Soc., Dalton Trans.* 2000; 577.
20. Gleizes AN. *Chem. Vapor. Depos.* 2000; **6**(4): 155.
21. Kodas TT, Hampden-Smith MJ (eds). *The Chemistry of Metal CVD*. VCH: Weinheim, 1998; 475.
22. Miyake H, Hayashi T and Sugiyama K. *J. Cryst. Growth* 1993; **134**: 174.
23. Shaukat A. *J. Phys. Chem. Solids* 1990; **51**: 1413.
24. Nomura R, Kanaya K and Matsuda H. *Chem. Lett.* 1988; **11**: 1849.
25. Nomura R, Fujii S, Kanaya K and Matsuda H. *Polyhedron* 1990; **9**: 361.
26. Nomura R, Sekl Y and Matsuda H. *J. Mater. Chem.* 1992; 765.
27. Nomura R, Sekl Y and Matsuda H. *Thin Solid Films* 1992; **209**: 145.
28. Hirpo W, Dhingra S, Sutorik AC and Kanatzidis MG. *J. Am. Chem. Soc.* 1993; **115**: 597.
29. Hollingsworth JA, Hepp AF and Buhro WE. *Chem. Vapor. Depos.* 1999; **5**: 105.
30. Hollingsworth JA, Buhro WE, Hepp AF, Jenkins PP and Stan MA. Spray chemical vapor deposition of $CuInS_2$ thin films for application in solar cell devices. In *Chemical Aspects of Electronic Ceramics Processing*, Kumta PN *et al.*, Materials Research Society Symposium Proceedings 495. MRS, Pittsburgh, PA. 1998: 171–176.
31. Harris JD, Hehemann DG, Cowen JE, Hepp AF, Raffaelle RP and Hollingsworth JA. Using single source precursors and spray chemical vapor deposition to grow thin-film $CuInS_2$. In *Proceedings of the 28th IEEE Photovoltaic Specialists Conference*, Anchorage, AK, 2000; 563–566.
32. Banger KK, Cowen J and Hepp AF. *Chem. Mater.* 2001; **13**(11): 3827.
33. Hollingsworth JA. Chemical routes to nanocrystalline and thin-film III–VI and I–III–VI semiconductors. PhD Thesis, Washington University, 1999; chapters 2 and 3.
34. Drago RS, Wong N, Bilgrien C and Vogel GC. *Inorg. Chem.* 1987; **26**: 9.
35. TA Instruments. Running experiments: preparing samples. In *Thermal Analysis & Rheology*, DSC 2920. Newcastle, DE, 1998; 11.
36. Cowen JE, Riga A, Hepp AF, Duraj S, Banger KK and MaClaron R. In *NATAS Conference Session: Thermal Application of Materials*, St Louis, MO, 2001.
37. Siemer K, Klaer J, Luck I and Braunig D. Influence of crystal

orientation on device performance of $CuInS_2$ solar cells. In *Proceedings of the 28th IEEE Photovoltaic Specialists Conference*, Anchorage, AK, 2000; 630–633.
38. Banger KK, Harris JD, Cowen JE and Hepp AF. In *E-MRS Spring Meeting, Symposium P: Thin Film Materials for Photovoltaics*, Strasbourg, France, 2001.
39. Albin D, Noufi R, Tuttle J, Goral J and Risbud SH. *J. Appl. Phys.* 1988; **64**: 4903.
40. Edington JW. *Practical Electron Microscopy in Materials Science.* Van Nostrand Reinhold: New York, 1976.
41. Soliman HS. *J. Phys. D: Appl. Phys.* 1998; **31**: 1516.
42. Scheer R, Diesner K and Lewerenz HJ. *Thin Solid Films* 1995; **268**: 130.
43. Tell B, Shay JL and Kasper HM. *J. Appl. Phys.* 1972; **43**: 2469.
44. Tiller WA. *Science* 1964; **146**: 871.
45. Jaffe JE and Zunger A. *Phys. Rev. B: Condens. Matter* 1983; **28**: 5176.

